http://doi.org/10.22364/ncmesc.06

6. Nanostructured TiO_2-based materials with photocatalytic properties

Nanostrukturēti TiO_2 materiāli un kompozīti ar fotokatalītiskām īpašībām

Ainārs Knoks, Līga Grīnberga, Jānis Kleperis, Ineta Liepiņa, Gunārs Bajārs

Institute of Solid State Physics, University of Latvia
Ķengaraga iela 8, Riga, LV-1063, Latvia
E-mail: *ainars.knoks@cfi.lu.lv*

Contents

6.1. Review of photocatalytic materials for water splitting

In order to reduce global climate change by limiting CO_2 emissions, it is necessary to switch from continuous power production by burning fossil fuels (coal, oil, gas) to the unsteady energy generation from local renewable energy sources. Wind, sun and rivers are the most popular renewable energy sources, but they are available occasionally or seasonally, which doesn't always coincide with required consumption. It is especially important for countries in Northern latitudes with dark and short days in winter, and sunny, long days in summer, like Latvia. Therefore, reliable energy storage systems are critically needed to store and supply power in continuous manner. Electricity and hydrogen are two comparable energy carriers, and in order to be able to meet humanity's demand for energy storage in the form of electricity and/or hydrogen, appropriate materials are researched [1]. In hydrogen economics, the production of hydrogen from renewables is very important.

TiO_2 has attracted high interest of industry and scientific communities. Following the discovery by Honda and Fujishima [2] of TiO_2 photocatalytic properties, it has been used

and investigated for wide variety of applications, such as, self-cleaning surfaces [3, 4] which was attributed to the size difference of the starting materials. The film with only 2 wt % TiO_2 maintained higher contact angle than the film without TiO_2 after 1800-h outdoor exposure, the accumulation of stain being avoided due to TiO_2 photocatalysis. The films prepared in this study are the first ones that satisfy the requirements of transparency, superhydrophobicity, and long lifetime simultaneously. Transparent superhydrophobic thin films with TiO_2 photocatalyst were prepared by utilizing a sublimation material and subsequent coating of a fluoroalkyl, water and air purification [5–9] scanning electron microscope-energy dispersive analysis of X-ray (SEM-EDAX) at the same time looking into the safety of TiO_2 [10] particularly under ultraviolet (UV) and as a viable energy harvesting solution via hydrogen production from water [11–13].

Due to its photocatalytic capability, low cost and chemically inert properties, TiO_2 is a promising material for water and air contamination treatment technologies [9, 14–16]. Most of investigations have been devoted to the pure TiO_2 films because of its reusability. However, practical application of such films is limited by fast recombination of photo-induced hole-electron pairs. Coupling TiO_2 with other inorganic oxides such as SiO_2 [17], SnO_2 [18], WO_3 [19], In_2O_3, (Sr, La)TiO_3, $ZnFe_2O_4$, and Fe_2O_3 [20] can increase the photon energy range of photo-excitation and this will change the photocatalytic efficiency [21].

Unfortunately, quantum yield for pristine TiO_2 is low, thus making photocatalytic hydrogen production from water not viable. To tackle this problem various modifications are performed. This chapter contains overview of used methods and practices of TiO_2 modifications.

TiO_2 has wide band gap that varies for polymorph phases, anatase has 3.2 eV, rutile 3.05 eV and brookite 3.4 eV [22]. Thus, TiO_2 can be excited only by UV light, that constitute about 10% of sun radiation, but only 5% reaches the surface of the Earth [23]. Indicating that either the quantum yield must be increased immensely, or absorption edge must be moved deeper into visible (VIS) range. Both directions are in the process of exploration due to benefits and downfalls.

Lowering the band gap of TiO_2 can be done through creation of heterostructure with narrow gap materials or doping with various materials. It has been reported that WO_3 increase of absorption in VIS region as shown by various research papers [19, 24–28].

Viable materials to lower TiO_2 band gap, for example nanowire TiO_2 wrapped with ZnO, reported lowering of band gap up to 2.6 eV [29]the impact of angstrom thick atomic layer deposited (ALD), or decorating TiO_2 nanotubes with Cu_2O particles shifting band gap into region of 1.5 to 3.3 eV [30]. Of course, other photoanode materials can be used to lower band gap and increase photocatalytic activity such as Fe_2O_3 thin film on anodized TiO_2 thus, enabling absorption of VIS light and increasing photocatalytic activity [31].

Doping of TiO_2 often brings increase of quantum yield at the same time changing band gap. Increase in yield can be due to additional levels that dopants bring or increase in generated charge carrier lifetime. Deposited CdS quantum dots increased charge carrier separation though additional conduction band (CB) electrons above CB edge of TiO_2 [32] or gold nanoparticle increase photocatalytic activity though localised surface plasmonic resonance and charge transfer kinetics [33]. Anionic and cationic doping is prominent choice for modifying TiO_2. N [34] and F [35] change the unit cell and crystallite size of anatase and rutile in addition to change of band gap. Combining S and N doping with graphene quantum dots modification increase hydrogen production, but again the proper

ratio is of great importance as showed by Xie et al. [36], where they investigated P25 doping with S,N-GQDs. At 3wt% providing highest yield.

Fe, C, V, and other dopants are possible [4]. Computational modelling of various dopants such as work by Lisovski et al. on various atom dopant influence on TiO_2 [37].

It is noteworthy that synthesis and treatment of TiO_2 is important, because various types of oxide perform differently. Anodized TiO_2 photocatalytic properties are annealing dependent, not only amorphous in comparison to crystalline but also annealing temperature dependent as it was shown by Macak [38].

All abovementioned efforts are to promote hydrogen generation through photocatalytic process. Change in band gap is important due to reduction dependency on the potential of generated charge carriers. Generated electrons in conduction band and hole in valence band then have to migrate to surface and interact with water molecule. This means band edge position can be crucial for efficient hydrogen production.

A detailed review by Jafari et al. shows that modifying TiO_2 brings various results for photocatalysis, from Pt, Cr, Ta doped TiO_2 producing 11.7 μmol h^{-1} to 647 mmol h^{-1} on Au-TiO_2 [39], thus, the investigation of sustainable and accessible photocatalyst is still in progress.

Thus, WO_3 is a suitable photo-electron storing material to couple with TiO_2 because WO_3 has narrower band gap (2.7 eV [40]) than that of TiO_2 to allow the transfer of photogenerated electrons from TiO_2 to ensure effective charge separation as shown in Fig. 6.1. As reported by [41] the ratio of WO_3 to TiO_2 is critical for higher photocatalytic activity with existing threshold of WO_3 coverage of TiO_2 surface for acquired photocurrent increase. Existence of threshold is set by generated charge carrier interfacial transfer, but over the threshold most of the light will be absorbed by WO_3 and as material with lower photocurrent values the result shows lower overall photocurrent. Authors suggest that generated e-h pairs go through charge interfacial transfer, hole from VB of WO_3 to VB of TiO_2 and e^- from TiO_2 CB to WO_3 CB [41].

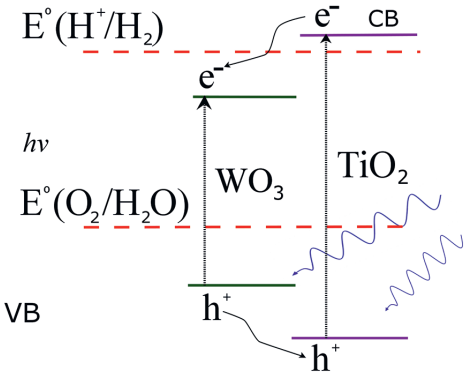

Figure 6.1. **Band structure of TiO_2/WO_3 heterosystem, optical absorption edge shift to VIS region**

In this chapter our research results on the role and properties of nanostructured TiO_2-based materials with photocatalytic properties have been summarized based on publications [28].

6.2. Methods applied to synthesize and research photocatalytic materials

There are chemical and physical thin film deposition techniques. Physical techniques include mechanical, electromechanical or thermodynamic processes, while chemical thin film deposition techniques usually involve a liquid precursor that forms a thin solid film as a result of a chemical reaction or indifferent solution with dispersed nanopowder of material. The most popular physical thin film deposition techniques are physical vapour deposition (resistive, inductive, electron beam, pulsed laser, arc-discharge, etc.) and sputtering techniques (direct current, alternating current, impulse, etc.). The most typical thick film growth techniques are electrochemical oxidation and deposition, electrophoretic deposition, spray pyrolysis, electrostatic spinning, spin coating and more. More detailed description of material synthesis methods used in this study will be described further.

Electrophoretic deposition (EPD) method is a highly beneficial, low-cost and eco-friendly technique for the preparation of required films and multi-layer coatings [42, 43]. For the electrophoretic growth two 3×3 cm^2 stainless steel (grade 316) electrodes were used. Distance between electrodes was 1 cm. A constant voltage of 100 V was applied between the electrodes by DC Power Supply (Agilent Technologies N5772A) and held for 10 min. EPD ensures colloidal particle deposition on substrate from electrically conductive electrolyte, in this case isopropanol. The process begins when applied electric field makes dispersed colloidal particles migrate to the electrode, where particles stay intact after losing charge. The deposited coatings were gradually heated (5 °C/min) and annealed at 500 °C for 2 h.

Electrophoretic deposition from suspension of TiO_2 : WO_3 mixtures (molar ratio in suspension 1 : 0, 1 : 1, 2 : 1, 3 : 1 and 1 : 2) in isopropanol (Fluka Analytical, 97%). To improve conductivity of dispersion media, pH of the suspension was adjusted with 1 mL HCl (Fluka Analytical, 98%). Each suspension was sonicated for 30 min. For the electrophoretic growth two 3×3 cm^2 stainless steel (grade 316) electrodes were used with distance 1 cm between them. A constant voltage of 100 V was applied to electrodes by DC Power Supply (Agilent Technologies N5772A) and held for 10 min. The deposited coatings were gradually heated (5 °C/min) and annealed at 500 °C for 2 h.

Electrochemical anodization. Coating of TiO_2 nanotube arrays were synthesized in electrochemical anodization using Ti foil (99.98% pure) and water-based electrolyte dissolving H_3PO_4 (Enola 96%) in deionized water. For anodization process to occur NaF was dissolved in electrolyte so that F^- ion wt% = 0.3, pH = 4 was adjusted by adding NaOH. Anodization was performed in two electrode cell (working electrode Ti foil, counter electrode – platinum plate, distance between electrodes 2.5 cm). Potential of 5 V was applied for 10 minutes, then anodization process was initiated at 20 V. After anodization samples were rinsed with deionized water and annealed in a muffle furnace at 500 °C for 120 minutes for crystallization of amorphous oxide. Then WO_3 was electro-phoretically deposited on TiO_2 surface from dispersed WO_3 in isopropanol/HCl using constant 120V potential with electrode separation of 2 cm. WO_3 was deposited on anodized samples at various stages before annealing and after annealing.

Analysis of material composition, structure and morphology. The structure of research materials was analysed by XRD (Diffractometer X'Pert Pro MPD, Cu anode, $\lambda = 0.154$ nm), morphology was studied by two different SEM systems (table-top device Phenom Pro up to 95000× magnification at 10 kV and SEM-FIB Tescan Lyra up to 30kV).

In addition, Raman spectroscopy was used (Renishaw InVia instrument with green laser (514 nm, max power 20 mW), objective ×100, laser power used 10%, 30–4000 cm^{-1} exposure time 10 s; red laser (633 nm, max power 12.5 mW) objective ×100, laser power used 10%, 30–4000 cm^{-1} exposure time 10 s).

Photocatalytic measurements were carried out using methylene blue (MB) solution under UV irradiation [28]. Each sample was placed in 80 mL of 0.43 mg/L MB solution in a quartz beaker and illuminated with Hg lamp from 30 cm distance. Each composite was used to obtain MB solution sample series after 0; 0.5; 1; 3 and 6 hours of photodegradation. Light absorption measurements (spectrophotometer Jenway 6300, 1 cm quartz cell) were used to calculate MB concentration after photodegradation had occurred.

Electrochemical photoactivity was determined using three electrode cell, where sample was used as working electrode, platinum (Pt) and calomel (SCE) respectively used as auxiliary and reference electrodes. Data were collected by potentiostat VoltaLab 40 (PGZ301 Radiometer analytical) in photoactivity measurements where the light source with 150 W xenon lamp, 10 mW/cm^2 was used. Photocurrent response (PCR), open circuit potential (OCP) measurements were performed in three electrode cell, sample as working electrode, Pt as auxiliary electrode and calomel as the reference electrode (SCE) was used in 1M NaOH.

6.3. Discussion about structure, composition and photo-electrochemical properties of TiO_2 – based materials

In this work multiple samples were created, Table 6.1 shows all samples discussed in this work.

Table 6.1. **Synthesized samples and synthesis parameters**

Mixed anodic/EPD samples					
Names	Composi-tion	Low voltage, V	Time, min	High voltage, V	Time, min
T1	TiO_2	5	15	20	90
TW1	TiO_2/WO_3	0	0	120	0
TW2	Ti/WO_3	0	0	120	6
T3	TiO_2	5	10	20	90
TW3	TiO_2/WO_3	0	0	120	6
T4	TiO_2	5	10	30	90
TW4	TiO_2/WO_3	0	0	0	0
T5	TiO_2	7	10	20	90
TW5	TiO_2/WO_3	0	0	120	8
TW6	TiO_2	0	0	120	6
TW7	TiO_2/WO_3	0	0	125	20
T8	TiO_2	5	15	20	90
TW8	TiO_2/WO_3	0	0	120	5

Samples obtained with EPD only					
Names	$m(TiO_2)$, g	$m(WO_3)$, g	$n(TiO_2)$, mol	$n(WO_3)$, mol	$n(TiO_2)$: $n(WO_3)$
a	1.55	4.52	0.019	0.019	1 : 1
b	3.07	4.52	0.038	0.019	2 : 1
c	4.71	4.52	0.059	0.019	3 : 1
d	1.51	8.96	0.019	0.039	1 : 2

Structure and morphology:

Phase composition and crystallinity were determined using XRD and Raman measurements. As shown in Fig. 6.2, EPD synthesized samples contain TiO_2 anatase peaks at 2θ = 25° (101) and 2θ = 25° (200). Similarly, anodic TiO_2 shows 2θ=25° (101) and well known three WO_3 peaks at 23.2 (002), 23.7 (020), and 24.5 (200). WO_3 crystallite size was determined to be from 35 to 64 nm, it was estimated using 2θ = 23°, whereas TiO_2 crystallite size was estimated to be 20 nm using 2θ = 25°, it done by using Scherrer equation [44].

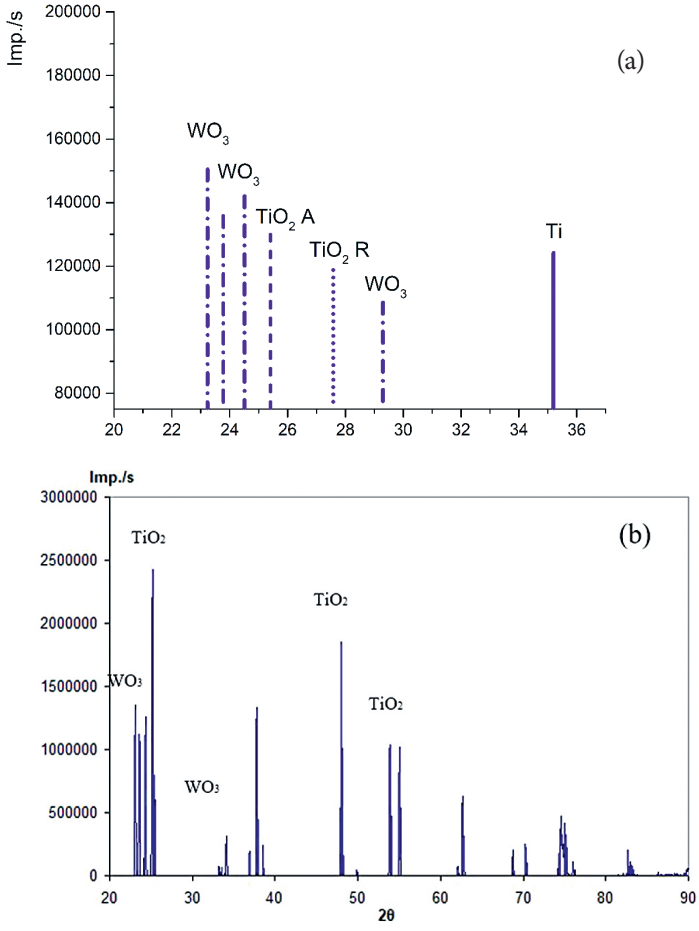

Figure 6.2. **XRD data for TiO_2/WO_3 samples a) anodic TiO_2 with EPD WO_3 sample TW8 b) EPD TiO_2/WO_3 sample d.**

Raman spectra indicates TiO_2 anatase and WO_3 presence, as seen in Fig. 6.3. EPD TiO_2/WO_3 showed anatase TiO_2 and WO_3 as expected, with bands at 150, 400, 515 and 633 cm^{-1} for TiO_2 and 274, 327, 716 and 806 cm^{-1} for WO_3. Though anodic TiO_2 with EPD WO_3 indicated bands at 144, 395, 516, 635 cm^{-1} and 57, 70, 132, 273, 716, 806 cm^{-1} for WO_3. Additionally, performing Raman mapping of the anodic/EPD sample surface for WO_3 particle distribution.

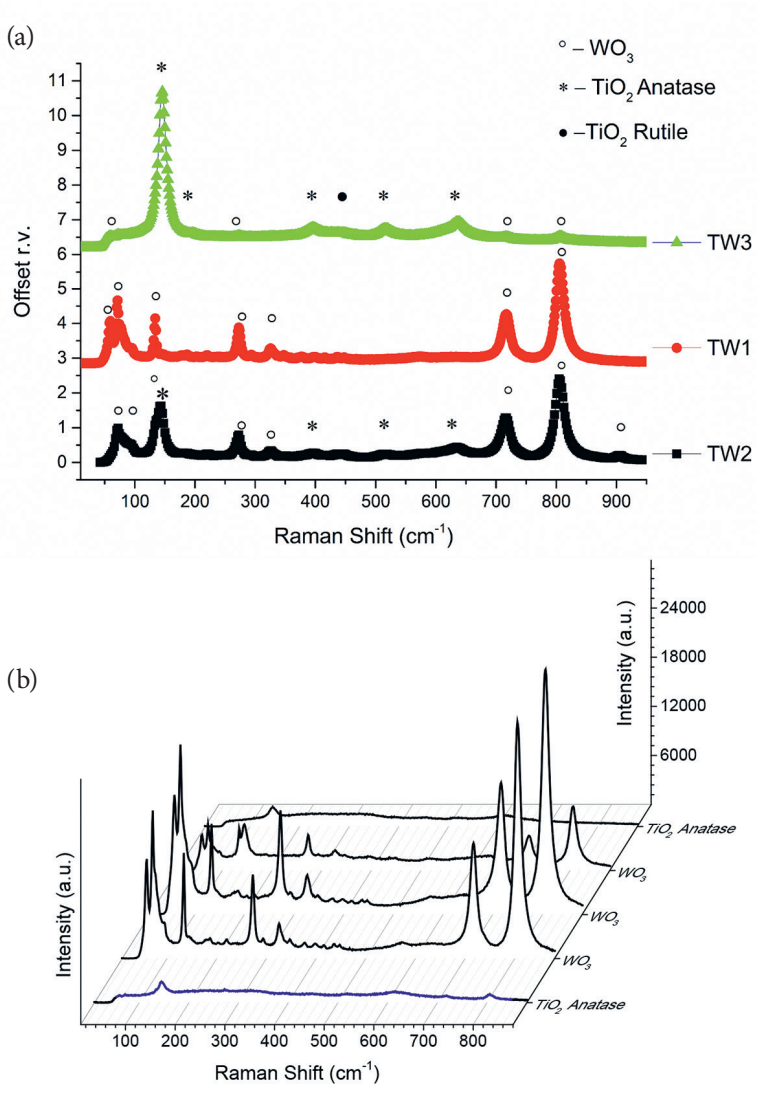

Figure 6.3. **Raman investigation of anodic TiO_2 with EPD WO_3. Clear anatase phase and WO_3 are present, as seen in image a), TW3 shows clear TiO_2, TW1 and TW2 is standard WO_3. Image b) Raman surface mapping of sample TW1, low intensity TiO_2 and higher intensity WO_3 bands indicate WO_3 particles on surface**

After comparison of results with known Raman band positions, it was noted that some TiO_2 and WO_3 bands are shifted compared to known values. That indicates a change in particle size after the heat treatment, thus, a probable change in band gap. Full comparison of measured band positions with known values is depicted in Table 6.2.

Table 6.2. **Characteristic Raman bands in vibration spectra of WO_3**

Band position, cm^{-1}	Vibrations*	Source
949	ν_s (W = O ter.)	[45]
806	ν_a (W–O–W)	[45]
801	"–"	[46]
805	"–"	[46]
806	"–"	[47]respectively, of well-defined W(VI
806	"–"	This work, sample TW1
806	"–"	Sample b
695	ν (W_2O_6&W_3O_8)	[45]
710	"–"	[45]
715	"–"	[46]
712	"–"	[47]respectively, of well-defined W(VI
716	"–"	This work, Sample TW1
716	"–"	Sample b
518	(O–Lattice)	[45]
316	(WO_3)	[45]
322	"–"	[46]
324		[46]
256	ν (O–W–O) δ (O–W–O)	[45]
262	"–"	[48]
270	"–"	[46]
270	"–"	[47]respectively, of well-defined W(VI
274	"–"	Sample b
272	"–"	This work, Samples TW1, TW2
194	W–W	[45]
180	"–"	[46]
130	"–"	[46]
76	"–"	Sample b
65	"–"	[45]

From SEM images self-organized TiO_2 tubes (Fig. 6.4 (a) and (b)) can be seen as well as deposited WO_3 on the surface as seen in Fig. 6.4 (c) and (d). In EPD samples, WO_3 showed 200 to 400 nm particles and similar results were gained for anodic/EPD samples.

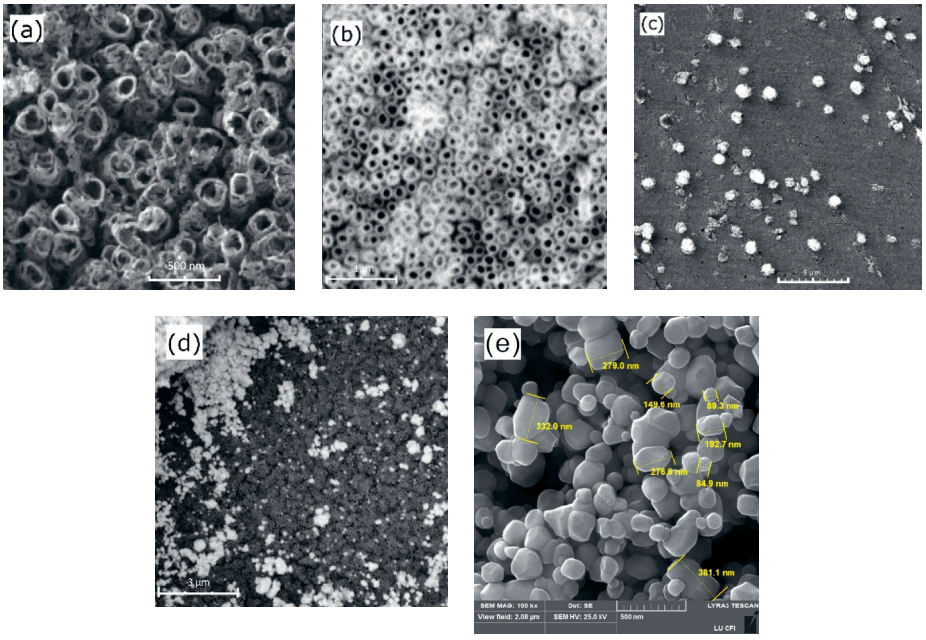

Figure 6.4. **SEM images of sample surface. (a) and (b) Anodic TiO_2 in tubular form, (d) and (c) TiO_2 surface after deposited WO_3, (e) EPD synthesized sample surface**

Photocatalytic activity was determined though MB degradation and photoelectrochemical properties such as photocurrent response, open circuit potential, EPD samples showed slower initial MB degradation as showed in Fig. 6.5 indicating that absorption and dissociation of water in contact with oxygen bridges, that is followed by oxide and superhydroxide species that performs the degradation of MB molecules. From MB degradation samples with resulting WO_3 content of 17.8%. With higher concentration WO_3 (19.9 wt%) MB degradation rate was lowest, thus showing that proper TiO_2/WO_3 ratio is crucial for highest photocatalytic properties.

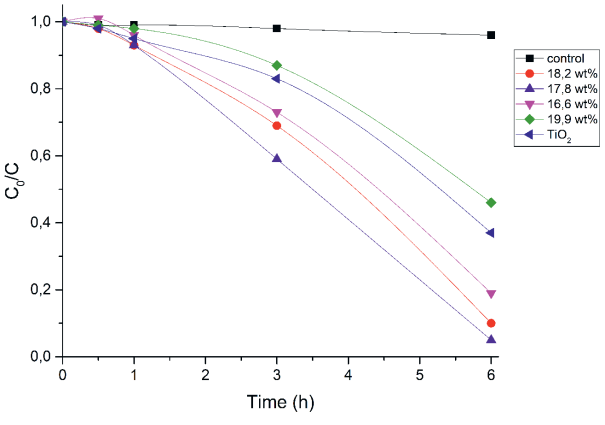

Figure 6.5. **MB degradation by EPD TiO_2/WO_3 mixture. Clear indication that proper ratio of WO_3 to TiO_2 for increase in photocatalytic activity**

Anodic samples also provided similar results, proper ratio is necessary for higher photocatalytic activity as indicated in Fig. 6.6 (a) and (c). Secondary heat treatment can lower photocatalytic activity, as seen in Fig. 6.6 (b), due to change in crystallite size and band gap as well as possible defect creation. Fig. 6.6 (c) show OCP comparison between various anodic TiO_2 with EPD WO_3, as one can see, the sample TW2 shows the highest potential in comparison to other samples.

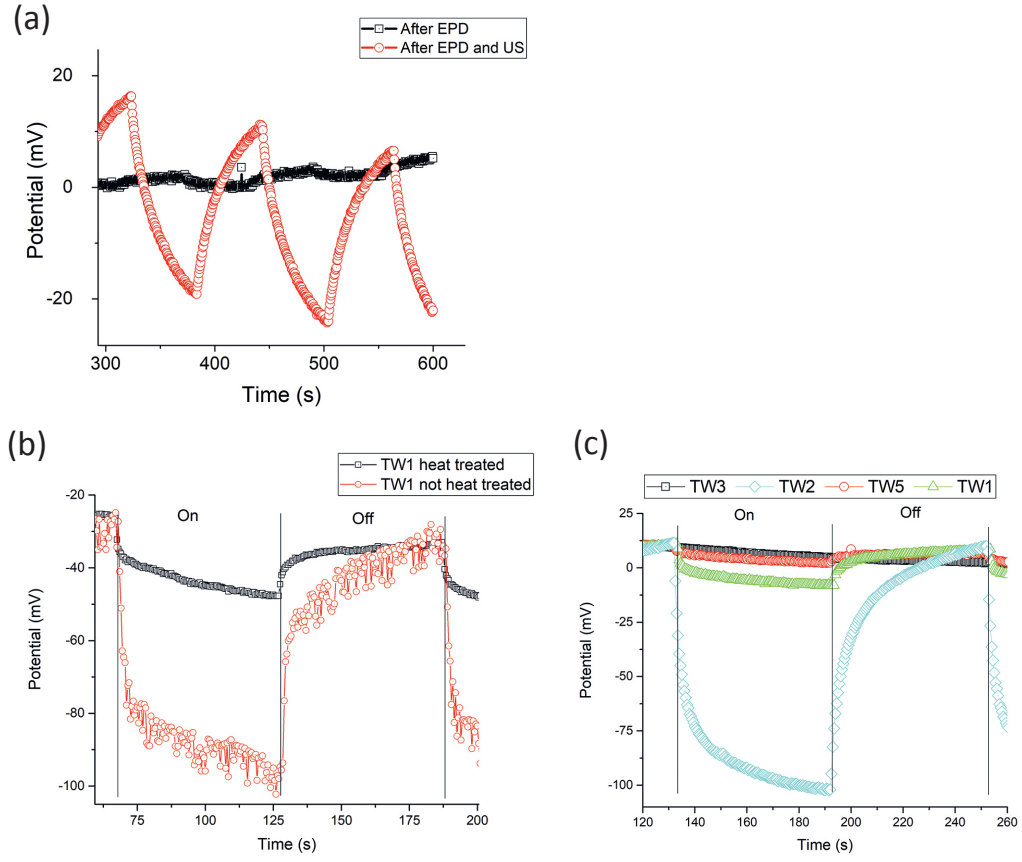

Figure 6.6. **OCP comparison for anodic TiO_2 samples with EPD WO_3. (a) proper TiO_2/WO_3 ration is necessary (b) additional heat treatment lowers OCP and thus photocatalytic activity (c) various anodic/EPD samples, sample with proper TiO_2/WO_3 ratio shows highest OCP value**

Investigation of optical band gap can be performed by finding absorption coefficient. Due to TiO_2 and WO_3 being deposited on non-transparent substrates absorption coefficient and optical band gap can be found from reflectance spectra using Kubelka-Munk transformation [49, 50]. As seen in Fig. 6.7, samples with WO_3 has lower optical absorption edge in comparison to only TiO_2 samples.

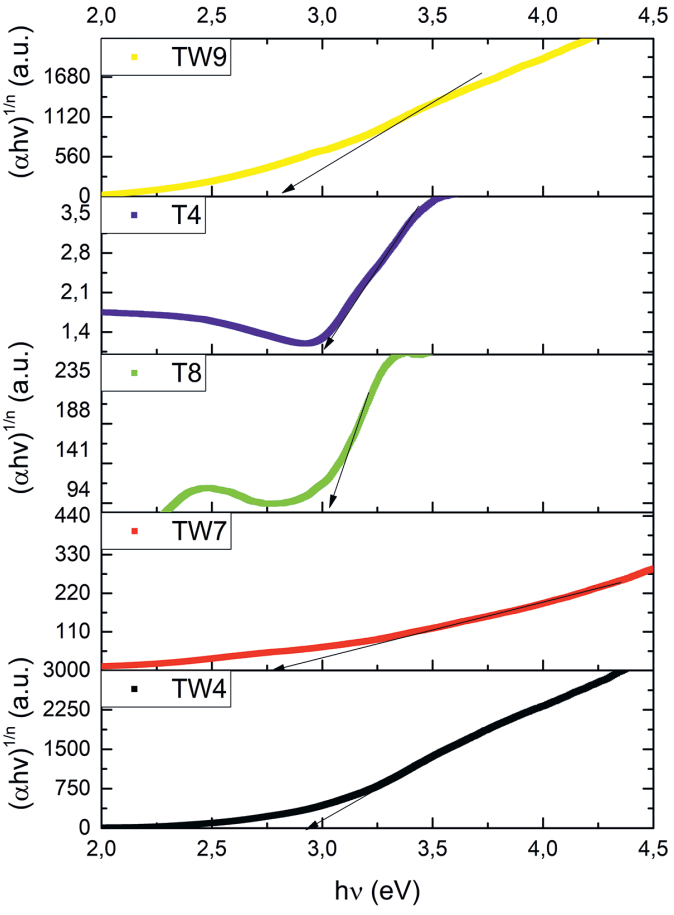

Figure 6.7. **Optical absorption edge determination through Kubelka-Munk transformation of reflectance spectra**

6.4. Conclusions

Investigation of two methodologies of photoanode synthesis was done through electrochemical anodization and electrophoretic deposition. Structural investigation indicated that after secondary heat treatment TiO_2 and WO_3 do not undergo phase transition. Upon further investigation Raman spectroscopy showed band position shifts that indicate change in particle size. Optical band gap investigation showed that combination of TiO_2 with WO_3 lowers band gap of material, coinciding with literature data. Secondary heat treatment might influence band gap size, but the influence is rather small.

Photocatalytic activity measurements clearly showed that TiO_2/WO_3 ratio directly influences photoactivity as by increasing of the WO_3 content photocatalytic activity also increases but after certain point it starts to decrease. Anodic TiO_2 with WO_3 showed similar results. In addition, secondary heat treatment lowered photoactivity, probably due to increased grain boundary or crystallite size change.

6.5. References

1. Züttel, A., Borgschulte, A. and Schlapbach, L. (eds.). (2008) Hydrogen as a future energy carrier. *Journal of Applied Electrochemistry*, 38(10), Wiley-VCH.
2. Fujishima, A. and Honda, K. (1972) Electrochemical Photolysis of Water at a Semiconductor Electrode. *Nature*, 238, 37–38.
3. Nakajima, A., Hashimoto, K., Watanabe, T., Takai, K., Yamauchi, G. and Fujishima, A. (2000) Transparent superhydrophobic thin films with self-cleaning properties. *Langmuir*, 16, 7044–7047.
4. Grimes, C. A. and Mor, G. K. (2009) *TiO_2 Nanotube Arrays*. Boston, MA: Springer US.
5. Oza, G., Pandey, S., Gupta, A., Shinde, S., Mewada, A., Jagadale, P., Sharon, M. and Sharon, M. (2013) Photocatalysis-assisted water filtration: using TiO_2-coated vertically aligned multi-walled carbon nanotube array for removal of Escherichia coli O157:H7. *Mater. Sci. Eng. C. Mater. Biol. Appl*., 33, 4392–4400.
6. Jamil, T. S., Ghaly, M. Y., Fathy, N. A., Abd El-Halim, T. A. and Österlund, L. (2012) Enhancement of TiO_2 behavior on photocatalytic oxidation of MO dye using TiO_2/AC under visible irradiation and sunlight radiation. *Sep. Purif. Technol*., 98, 270–279.
7. Tang, Y., Luo, S., Teng, Y., Liu, C., Xu, X., Zhang, X. and Chen, L. (2012) Efficient removal of herbicide 2,4-dichlorophenoxyacetic acid from water using Ag/reduced graphene oxide co-decorated TiO_2 nanotube arrays. *J. Hazard. Mater*., 241–242, 323–330.
8. Houas, A. (2001) Photocatalytic degradation pathway of methylene blue in water. *Appl. Catal. B. Environ*., 31, 145–157.
9. Pichat, P. (2013) *Photocatalysis and Water Purification: From Fundamentals to Recent Applications*. Wiley, 438 pages, ISBN: 978-3-527-33187-1
10. Sayes, C. M., Wahi, R., Kurian, P. A., Liu, Y., West, J. L., Ausman, K. D., Warheit, D. B. and Colvin, V. L. (2006) Correlating nanoscale titania structure with toxicity: A cytotoxicity and inflammatory response study with human dermal fibroblasts and human lung epithelial cells. *Toxicol. Sci*., 92, 174–185.
11. Fujishima, A., Zhang, X. and Tryk, D. (2008) TiO_2 photocatalysis and related surface phenomena. *Surf. Sci. Rep.,* 63, 515–582.
12. Fujishima, A., Rao, T. N. and Tryk, D. A. (2000) Titanium dioxide photocatalysis 1, *Journal of Photochemistry and Photobiology C Photochemistry Reviews*, 1–21.
13. Young, K. J., Martini, L., Milot, R. L., Snoeberger, R. C., Batista, V. S., Schmuttenmaer, C., Crabtree, R. H., Brudvig, G. W., (2012) Light-driven water oxidation for solar fuels. *Coord. Chem. Rev*., 256, 2503–2520.
14. Ilie, M., Cojocaru, B., Parvulescu, V. I. and Garcia, H. (2011) Improving TiO_2 activity in photo-production of hydrogen from sugar industry wastewaters. *Int. J. Hydrogen Energy*, 36, 15509–15518.
15. Serrano, B. and de Lasa, H. (1997) Photocatalytic Degradation of Water Organic Pollutants. Kinetic Modeling and Energy Efficiency. *Ind. Eng. Chem. Res*., 36, 4705–4711.
16. Rajeshwar, K., Osugi, M. E., Chanmanee, W., Chenthamarakshan, C. R., Zanoni, M. V. B., Kajitvichyanukul, P. and Krishnan-Ayer, R. (2008) Heterogeneous photocatalytic treatment of organic dyes in air and aqueous media. J. Photochem. Photobiol. *C Photochem. Rev*., 9, 171–192.
17. Wang, J., Yang, G., Lyu, W. and Yan, W. (2016) Thorny TiO_2 nanofibers: Synthesis, enhanced photocatalytic activity and supercapacitance. *J. Alloys Compd*., 659, 138–145.
18. Abdullah, H., Khan, M. M. R., Ong, H. R. and Yaakob, Z. (2017) Modified TiO_2 photocatalyst for CO_2 photocatalytic reduction: An overview. *J. CO_2 Util*., 22, 15–32.
19. Li, X. Z., Li, F. B., Yang, C. L. and Ge, W. K. (2001) Photocatalytic activity of WO_x-TiO_2 under visible light irradiation. *J. Photochem. Photobiol. A Chem*., 141, 209–217.
20. Šutka, A., Vanags, M., Joost, U., Šmits, K., Ruža, J., Ločs, J., Kleperis, J. and Juhna, T. (2018) Aqueous synthesis of Z-scheme photocatalyst powders and thin-film photoanodes from earth abundant elements. *J. Environ. Chem. Eng*., 6, 2606–2615.

21. Georgieva, J., Valova, E., Armyanov, S., Philippidis, N., Poulios, I. and Sotiropoulos, S. (2012) Bi-component semiconductor oxide photoanodes for the photoelectrocatalytic oxidation of organic solutes and vapours: A short review with emphasis to TiO_2-WO_3 photoanodes. *J. Hazard. Mater.*, 211–212, 30–46.
22. Edelmannová, M., Lin, K. Y., Wu ,J. C. S., Troppová, I., Čapek, L. and Kočí, K. (2018) Photocatalytic hydrogenation and reduction of CO_2 over CuO/ TiO_2 photocatalysts. *Appl. Surf. Sci.*, 454, 313–318.
23. Nunez, M., Forgan, B. and Roy, C. (1994) Estimating ultraviolet radiation at the earth's surface. *Int. J. Biometeorol.*, 38, 5–17.
24. Nazari, M., Golestani-Fard, F., Bayati, R. and Eftekhari-Yekta, B. (2015) Enhanced photocatalytic activity in anodized WO_3-loaded TiO_2 nanotubes. *Superlattices and Microstruct.*, 80, 91–101.
25. Kmentova, H., Kment, S., Wang, L., Pausova, S., Vaclavu, T., Kuzel, R., Han, H., Hubicka, Z., Zlamal, M., Olejnicek, J., Cada, M., Krysa, J. and Zboril, R. (2016) Photoelectrochemical and structural properties of TiO_2 nanotubes and nanorods grown on FTO substrate: Comparative study between electrochemical anodization and hydrothermal method used for the nanostructures fabrication. *Catal. Today*, 287, 130–136.
26. Ashokkumar, M. (1998) An overview on semiconductor particulate systems for photoproduction of hydrogen. *Int. J. Hydrogen Energy*, 23, 427–438.
27. Anandan, S., Sivasankar, T. and Lana-Villarreal, T. (2014) Synthesis of TiO_2/WO_3 nanoparticles via sonochemical approach for the photocatalytic degradation of methylene blue under visible light illumination. *Ultrason. Sonochem.*, 21, 1964–1968.
28. Liepina, I., Bajars, G., Rublans. M., Kleperis, J., Lusis, A. and Pentjuss, E. (2015) Structure and Photocatalytic Properties of TiO_2 -WO_3 Composites Prepared by Electrophoretic Deposition. *IOP Conf. Ser. Mater. Sci. Eng.*, 77, 012039.
29. Ghobadi, A., Ulusoy, T. G., Garifullin, R., Guler, M. O. and Okyay, A. K. (2016) A heterojunction design of single layer hole tunneling ZnO passivation wrapping around TiO_2 nanowires for superior photocatalytic performance. *Sci. Rep.*, 6, 30587.
30. Jagminas, A., Kovger, J., Rėza, A., Niaura, G., Juodkazytė, J., Selskis, A., Kondrotas, R., Šebeka. B. and Vaičiūnienė, J (2014) Decoration of the TiO_2 nanotube arrays with copper suboxide by AC treatment. *Electrochim. Acta*, 125, 516–523.
31. Cong, Y., Li, Z., Zhang, Y., Wang, Q. and Xu, Q. (2012) Synthesis of Fe_2O_3/TiO_2 nanotube arrays for photoelectro-Fenton degradation of phenol. *Chem. Eng. J.*, 191, 356–363.
32. Zhao, D. and Yang, C.-F. (2016) Recent advances in the TiO_2/CdS nanocomposite used for photocatalytic hydrogen production and quantum-dot-sensitized solar cells. *Renew. Sustain. Energy Rev.*, 54, 1048–1059.
33. Haro, M., Abargues, R., Herraiz-Cardona, I., Martínez-Pastor, J. and Giménez, S. (2014) Plasmonic versus catalytic effect of gold nanoparticles on mesoporous TiO_2 electrodes for water splitting. *Electrochim. Acta*, 144, 64–70.
34. Rumaiz, A. K., Woicik, J. C., Cockayne, E., Lin, H. Y. and Jaffari, G. H. (2009) Oxygen vacancies in N doped anatase TiO_2: Experiment and first-principles calculations. *Applied Physics Letters*, 95(26), Article ID 262111, 6–9.
35. Samsudin, E. M. and Abd Hamid, S. B. (2017) Effect of band gap engineering in anionic-doped TiO_2 photocatalyst. *Appl. Surf. Sci.*, 391, 326–336.
36. Wang, W., Zhou, Q., Fei, X., He, Y., Zhang, P., Zhang, G., Peng, L. and Xie, W. (2010) Synthesis of CuO nano- and micro-structures and their Raman spectroscopic studies. *Cryst. Eng. Comm.*, 12, 2232–2237.
37. Lisovski, O., Chesnokov, A., Piskunov, S., Bocharov, D., Zhukovskii, Y. F., Wessel, M. and Spohr, E. (2016) Ab initio calculations of doped TiO_2 anatase (101) nanotubes for photocatalytical water splitting applications. *Mater. Sci. Semicond. Process.*, 42, 138–141.
38. Macak, J. M., Gong, B. G., Hueppe, M. and Schmuki, P. (2007) Filling of TiO_2 nanotubes by self-doping and electrodeposition. *Adv. Mater.*, 19, 3027–3031.

39. Jafari, T., Moharreri, E., Amin, A., Miao, R., Song, W. and Suib, S. (2016) Photocatalytic Water Splitting – The Untamed Dream: *A Review of Recent Advances. Molecules*, 21, 900.
40. González-Borrero, P. P., Sato, F., Medina, A. N., Baesso, M. L., Bento, A. C., Baldissera, G., Persson, C., Niklasson, G. A., Granqvist, C. G. and Ferreira Da Silva, A. (2010) Optical band-gap determination of nanostructured WO_3 film. *Appl. Phys. Lett.*, 96, 4–6.
41. Qamar, M., Drmosh, Q., Ahmed, M. I., Qamaruddin, M. and Yamani, Z. H. (2015) Enhanced photoelectrochemical and photocatalytic activity of WO_3-surface modified TiO_2 thin film. *Nanoscale Res. Lett.*, 10, 54.
42. Besra, L. and Liu, M. (2007) A review on fundamentals and applications of electrophoretic deposition (EPD). *Prog. Mater. Sci.*, 52, 1–61.
43. Djošić, M. S., Miskovic-Stankovic, V. B., Janaćković, D .T., Kačarević-Popović, Z. M. and Petrović, R. D. (2006) Electrophoretic deposition and characterization of boehmite coatings on titanium substrate. *Colloids Surfaces A Physicochem. Eng. Asp.*, 274, 185–191.
44. Patterson, A. L. (1939) The Scherrer Formula for X-Ray Particle Size Determination. *Phys. Rev.*, 56, 978–982.
45. Díaz-Reyes, J., Dorantes-García, V., Pérez-Benítez, A. and Balderas-López, J. A. (2008) Obtaining of films of tungsten trioxide (WO_3) by resistive heating of a tungsten filament. *Superf. y Vacío*, 21, 12–17.
46. Diaz-Reyes, J., Flores-Mena, J. E., Gutierrez-Arias, J. M., Morin-Castillo, M. M., Azucena-Coyotecatl, H., Galván, M., Rodriguez-Fragoso, P. and Mendez-López, A. (2010) Optical and structural properties of WO_3 as a function of the annealing temperature. In: Frazao, O. (ed.). Sensig Materials. Proceedings of the 3rd WSEAS International Conference on Advances in Sensors, *Signals and Materials*, 99–104.
47. Ross-Medgaarden, E. I. and Wachs, I. E. (2007) Structural Determination of Bulk and Surface Tungsten Oxides with UV-vis Diffuse Reflectance Spectroscopy and Raman Spectroscopy. *J. Phys. Chem. C*, 111, 15089–15099.
48. Choi, H. C., Jung, Y. M. and Kim, S. Bin. (2005) Size effects in the Raman spectra of TiO_2 nanoparticles. *Vib. Spectrosc.*, 37, 33–38.
49. Kubelka, P. (1948). New Contributions to the Optics of Intensely Light-Scattering Materials Part I. *J. Opt. Soc. Am.*, 38, 448.
50. Kubelka, P. (1954) New Contributions to the Optics of Intensely Light-Scattering Materials Part II: Nonhomogeneous Layers. *J. Opt. Soc. Am.*, 44, 330.

6.6. Kopsavilkums

Lai risinātu pasaules enerģijas iegūšanas un izmantošanas problēmas, kā arī pārietu uz ilgtspējīgiem un videi draudzīgiem risinājumiem, tiek meklēti atjaunojami energoresursi un jaunas tehnoloģijas. Kā viens no daudzsološiem risinājumiem ir fotokatalītisku materiālu izmantošana gaisa, ūdens attīrīšanai, kā arī enerģijas iegūšanai un uzglabāšanai ūdeņraža formā, kur ūdeņradi iespējams iegūt, fotokatalītiski sadalot ūdeni. Tiek meklēti dažādi materiāli šīs funkcijas veikšanai, piemēram, titāna dioksīds (TiO_2), volframa trioksīds (WO_3), dzelzs oksīdi, kadmija selenīds (CdS), vara oksīdi, cinka oksīds un citi. Fotokatalīzes procesā svarīgu vietu ieņem materiāla aizliegtās zonas platums, tam jābūt pēc iespējas šaurākam, lai iekļautos redzamās gaismas diapazonā, jo līdz Zemes virsmai nonāk 3–5% no UV starojuma (kurā darbojas lielākā daļa fotokatalītiski aktīvo materiālu), bet redzamā gaisma ir 40%. TiO_2 ir viens no daudzsološiem fotokatalizatoriem, tas ir fotoķīmiski izturīgs, relatīvi vienkārši iegūstams, bet tā absorbcijas mala ir UV diapazonā.

Kombinējot dažādus materiālus, iespējams iegūt fotokatalizatoru ar mazāku absorbcijas malu un lielāku fotokatalītisko aktivitāti, piemēram, TiO_2/WO_3. Šajā darbā tiek dots pārskats par heterostruktūru un tās fizikālajām un fotoķīmiskajām īpašībām.

Tika izveidotas divas paraugu sērijas – viena, lietojot TiO_2 un WO_3 pulverus dažādās attiecībās (a, b, c, d paraugs). Otra – elektroķīmiski audzētas TiO_2 nanostruktūras, kurām uzklāts WO_3 pulveris. Pulveru uzklāšanu veikta ar elektroforēzes metodi (EPD).

Paraugu morfoloģija tika pētīta ar skenējošo elektronu mikroskopu (SEM). Strukturālās īpašības tika noteiktas, lietojot rentgenstaru difrakciju (XRD) un Ramana spektroskopiju. Optiskās īpašības pētītas, lietojot difūzo atstarošanos un Kubelkas–Munka transformāciju. Savukārt fotokatalītiskās īpašības noteiktas, izmantojot atvērtās ķēdes potenciāla (OCP), fotostrāvas (PCR) un metilēnzilā sadalīšanās mērījumus.

Morfoloģijas pētījumi atklāja, ka, izmantojot EDP metodi, WO_3 (redzami 6.4. e attēlā) ir uzklāts vienmērīgā kārtā uz TiO_2 virsmas ar daļiņu izmēru 200 līdz 400 nm, savukārt anodēts TiO_2 (redzams 6.4. a attēlā) atklāja pašorientētu nanocauruļu morfoloģiju ar daudz lielāku aktīvo virsmu. Gan tikai EPD metodē iegūtās TiO_2/WO_3 kārtiņas, gan arī anodēts TiO_2 ar EPD metodē uzklātu WO_3 uzrāda abu oksīdu esamību uz virsmas, pirmajā gadījumā – vienmērīgs daļiņu sadalījums uz pamatnes un otrajā gadījumā – atsevišķas WO_3 daļiņas uz virsmas. SEM mērījumi pierāda, ka WO_3 uznešanas laikā iespējams pārklāt visu TiO_2 virsmu, samazinot kopējo aktīvās virsmas laukumu, tādējādi samazinot kompozīta fotoaktivitāti. Šie mērījumi apliecina, ka fotokatalītisko īpašību uzlabošanai nepieciešams izmantot optimālu oksīdu attiecību.

Struktūras pētījumi uzrādīja, ka visi paraugi satur kristāliskās fāzes TiO_2 un WO_3. Pārsvarā TiO_2 tika iegūts anatāza fāzē, ko apstiprina zinātniskās literatūras un empīriskie dati – karsējot TiO_2 līdz 500 °C, fāžu pāreja anatāzs-rutils vēl nenotiek. Novērtējot XRD datus, tika noteikts raksturīgais kristalītu izmērs – WO_3 35 līdz 64 nm un TiO_2 ap 20 nm. Tika novērots, ka atkārtotas karsēšanas gadījumā WO_3 notiek Ramana pīķu pārbīde (skatīt apkopotos rezultātus 2. tabulā). Nobīde var būt saistīta ar kristalītu lieluma izmaiņu vai karsēšanas rezultātā iegūtiem skābekļa nestehiometrijas defektiem. Precīza mehānisma noskaidrošanai jāveic tālāka izpēte.

Fotokatalītisko īpašību pētījumi skaidri parāda, ka ir optimāla oksīdu daudzumu attiecība, pie kuras iegūst fotokatalītiskās aktivitātes pieaugumu. Nesasniedzot un pārsniedzot šo lielumu, aktivitāte pie noteiktiem apstākļiem, piemēram, aizsegtas TiO_2 virsmas vai liela robežvirsmas laukuma, kļūst mazāka nekā tīram TiO_2, kā tas ir redzams 6.5. un 6.6. attēlā. Tika arī noskaidrots aizliegtās zonas platums (6.7 attēls), kas apstiprināja absorbcijas malas pārbīdi no 3.2 eV TiO_2 paraugiem uz 2.7–2.8 eV kompozītam TiO_2/WO_3.

Savienojot TiO_2 ar WO_3, iespējams pārbīdīt optiskās absorbcijas malas novietojumu redzamās gaismas diapazonā, tādējādi palielinot materiāla fotokatalītiskās īpašības. Savukārt, veidojot fotokatalizatoru, nepieciešams atrast un optimizēt abu oksīdu daudzumu attiecību augstākās aktivitātes iegūšanai.